Microscopic Examination and Elemental Analysis of Field Emission Sites in 5.8 GHz Superconducting Mushroom Cavities*

T. Hays, M. Klauda†, J. Knobloch, D. Moffat, and H. Padamsee
Laboratory of Nuclear Studies, Cornell University, Ithaca, NY 14853

S. Durbin and M. Gray‡
Carleton College, Northfield, MN 55057

Abstract

Studies of RF field emission in a superconducting Nb "mushroom" cavity ($\sim$ 5.8GHz) were performed. Peak electric fields up to 98 MV/m have been achieved so far in this cavity with a demountable endplate. The demountable endplate allowed us to examine the regions exposed to the highest fields using an Scanning Electron Microscope (SEM), Energy Dispersive x-ray Spectroscopy(EDS), Auger Electron Spectroscopy (AES), and an Atomic Force Microscope (AFM). Through AES we found an impurity in every emission site. Also was discovered that "starbursts" correspond to areas of depleted fluorine on the Nb surface. AFM yielded more detailed information on the exotic topology of the former emission sites.

*Work supported by the National Science Foundation and the US-Japan collaboration
†Present address: Phys. Inst. III, D-W8520 Erlangen, Germany
‡Present address: Dept. of Physics, University of Virginia, Charlottesville, VA 22901

Introduction

In order to examine RF field emission sites we use a "Mushroom" cavity, a niobium cavity with an endplate having an inward indentataion, or dimple, which produces a geometric field enhancement in a region 1.25cm across. A review of previous studies with the mushroom cavity has been done by Moffat et al.[1] A demountable endplate containing the dimple allowed us to examine easily a cavity surface following an RF test. Following an RF test, the 15cm plate is removed and the high field region is examined in a Scanning Electron Microscope (SEM). So far a maximum electric field of 98MV/m at the dimple has been achieved with this cavity with a demountable endplate.

Starbursts, $50 - 200\mu$m starshaped regions of reduced secondary electron emission coefficient, are used to aid in locating the sites where we believe field emission activity has occured. Molten craters are usually found at the center of the starburst and are often accompanied by ripples, concentric ring patterns with a separation of 300nm.

For examination of these Nb surfaces we have an in-house SEM equipped with an energy dispersive x-ray spectroscopy (EDS) system for elemental analysis. With EDS we were able to detect impurities within the starbursts in only about 50% of the sites. For us this raised an interesting and important question. Are there impurities present which are not being detected by the EDS, for instance surface impurities much less than 0.1μm (the approximate depth limit of x-ray production[2]) deep? Or are there indeed sites which have no impurity and still emitted during the RF test with the aid of some other mechanism? To answer this question we conducted Auger Electron Spectroscopy (AES) analysis[1] on four sample plates (labeled XX, S-200, N1, and N2).

Starbursts

Experience shows that an atmospheric exposure on the order of several hours causes most starbursts to fade away, but the topological features such as the craters remain unchanged. Starbursts have shown themselves to be stable in vacuum and in a dry nitrogen atmosphere. Surprisingly, we observed starbursts to survive a CO_2 "snow cleaning" treatment [2]. We were not able to observe starbursts under an optical microscope (see Figure 1) but they

[1] AES was done at the lab of Evans East, Inc. in Plainsboro, NJ.

[2] Snow cleaning is a surface cleaning procedure using a jet of solid and gaseous CO_2.

can be observed by Secondary Electron Imaging (SEI) and through the use of absorbed current detection.

It might be significant to note that we had great difficulty observing the starbursts in the AES system at the Evans East lab using the associated SEI system, but we were subsequently able to observe them again in our lab. Just what differences in the equipment caused this is yet unclear.

Surface Fluorine

Using AES we compared spectra, Figure 2, just inside and just outside a starburst fringe "track" on sample XX. We found fluorine off the starburst track but no fluorine inside the track. An AES fluorine map on a random region off the dimple of sample N1 showed varying amounts of fluorine in a 300μm by 200μm region. No systematic depth profiling was done but from two argon sputterings of the surface we can remark that the fluorine layer in the region of interest of N1 was at least 50Å but not more than 1500Å deep. Fluorine presumably comes from the HF in the acid etching solution (BCP 1:1:2) used preparing the Nb surface for RF testing.

Figure 3 shows a fluorine map and a reference SEI photo including a starburst on a third sample N2. The starburst is observed to correspond to regions of fluorine depletion. The phenomenon which produced the starburst apparently acted to remove fluorine. There still exists the question whether the absence of fluorine alone is enough to produce the change in secondary electron coefficient observed in an SEM or whether other processes are at work.

Natural Emitters

To look for the cause of naturally occuring field emitters, Auger spectroscopy analyses were done on 29 central craters (25 on one plate and 4 on another), and impurities were detected in 100% of them. The incidence of these impurities is shown in Figure 4. Iron, chromium, and silicon were found to be the most common impurities. When iron was found, chromium was often found as well suggesting that stainless steel was the source.

Among the other inpurities found were Ni, Mn, In, Cu, C, F, Cl, and Mg. Carbon and oxygen were found over the entire surface as expected due to airborne hydrocarbons and their presence as impurities was recorded only when their concentrations were clearly above background.

Upon returing to Cornell, a further SEM study of these Auger analyzed

sites was performed but for most of the sites, the low impurity concentration and/or shallow depth caused the foreign elements found by AES to be at or below the limit of the EDS system. This confirms the suspicion that EDS is not the ideal tool for detecting impurities at former emission sites.

For every one of the central craters scanned in the Auger system, a featureless point ($\sim$ 500nm diameter) near ($5-30\mu$m distant) the central crater was also scanned. Surprisingly the featureless point often contained the impurities as well. Iron, for instance, was likely to be found as far out as six times the radius of the central crater. Indeed in six out of thirteen of those cases the concentration of impurity at the featureless point was greater than that found in the central crater. The concentration was seen to decrease thereafter to zero.

Figure 5 gives a specific example of the iron distribution by an Auger map and its corresponding SEI. The iron is seen to be localized to the region of a crater yet the edge of the crater does not provide a discrete boundary to the impurity concentration. Also note that iron is present in only one crater. No impurity was detected in the second crater of Figure 5.

Craters within a starburst other than the central crater we refer to as satellite craters. We found that in the ten satellite craters examined with AES on assorted sites, only two had impurities. These two were very close to the central crater making it plausable that the presence of impurities in these two is due to the distributed impurity of the central crater. The question remains that if these satellite craters are generally free from impurities, what role do they play in the explosive field emission event?

AFM Examination

Atomic Force Microscopy (AFM) images were obtained from a mushroom cavity dimple region that had been shown by electron microsocpy to have a cratered region surrounded by ripples. This region is shown in Figure 6. The sample was imaged in air; preparation involved only blowing with an air jet to remove loose contaminants.

With the topographical imaging capability of the AFM, the large craters at the center are found to be depressions $\sim 1\mu$m deep, with a raised edge about equally high. In diameter they range from $0.2-2\mu$m. Craters towards the periphery of a cluster are of smaller dimensions. The edge is irregular, having rounded projections reminiscent of the splash from a disturbed fluid. Much of the crater surface is smooth, but in places there appear to be

modulations similar to the ripples described below.

Also prominant as topographical features are the wavetrains, or ripple patterns, which are unquestionably the patterns seen at lower resolution in the SEM (Figure 6). They generally seem to emanate from a point near, but not exactly at, a peripheral crater, and propagate on the order of 100μm. Ripples from different sources seem not to interfere, but to form distinct domains with smooth boundaries (see Figure 7).

In general, there is a gradual decrease in wavelength with distance from the center, but the wavelength may vary in different directions even within a small region. The range of wavelengths on the sample studied was about 200nm to 650nm. The wave profile was nearly sinusiodal in some regions, but quite different in others. Crest-to-trough amplitudes were in the range of 10nm to 35nm, with higher amplitudes nearer the source.

We found one example of a wavetrain generated at a site $\sim$ 30μm from the nearest crater of the central cluster (see Figure 8). The concentric ripples, having a peak-to-peak amplitude of $\sim$ 30nm, are best described as nearly circular ellipses with a common focus, at which is found a bump $\sim$ 100nm high. The wave profile is far from sinusoidal, as indicated in Figure 8.

In some regions, especially nearer the craters, the crests of the ripples seem to break up into nodules, in a manner reminiscent of surface tension effects in liquids. An example of this effect (not near a crater) can be seen in Figure 7. In these regions, the wave profile is also different: wavelengths tend to be longer (up to 600 nm), the crests relatively narrow, and the troughs wide and rather flat.

Conclusions

That we found impurities in 100% of the sites we examined using AES supports the idea that field emission is caused predominantly by the presence of some impurity. The approach suggested by this result is that the surface needs to be cleaner to reduce the incidence of field emission. The elemental impurities found in this study are not inconsistent with the contaminants that one may find in the clean room cavity assembly environment. The metals may come from steel bolts and other metal assembly pieces. Possibly the silicon may even come from the borosilicate glass found in the high efficiency particulate air (HEPA) filters.[4]

References

[1] D. Moffat, P. Barnes, T. Flynn, J. Graber, L. Hand, W. Hartung, T. Hays, J. Kirchgessner, J. Knobloch, R. Noer, H. Padamsee, D. Rubin, and J. Sears, *Particle Accelerators*, **40**, pp.85-126, 1992.
and D. Moffat et al. *Proc. of the 5th Workshop on RF Superconductivity*, DESY, Hamburg, pp. 245-284, 1991.

[2] D. Moffat, internal Cornell SRF note SRF901012/11 and references therin.

[3] R. Moore, Evans East, Inc., private communication.

[4] F.A. Stevie, E.P. Martin,Jr., P.M. Kahora, J. T. Cargo, A.K. Nanda, A.S. Harrus, A.J. Muller, and H. W. Krautter, *J. Vac. Sci. Technol. A*, **9**, 5, pp. 2813-2816, 1991.

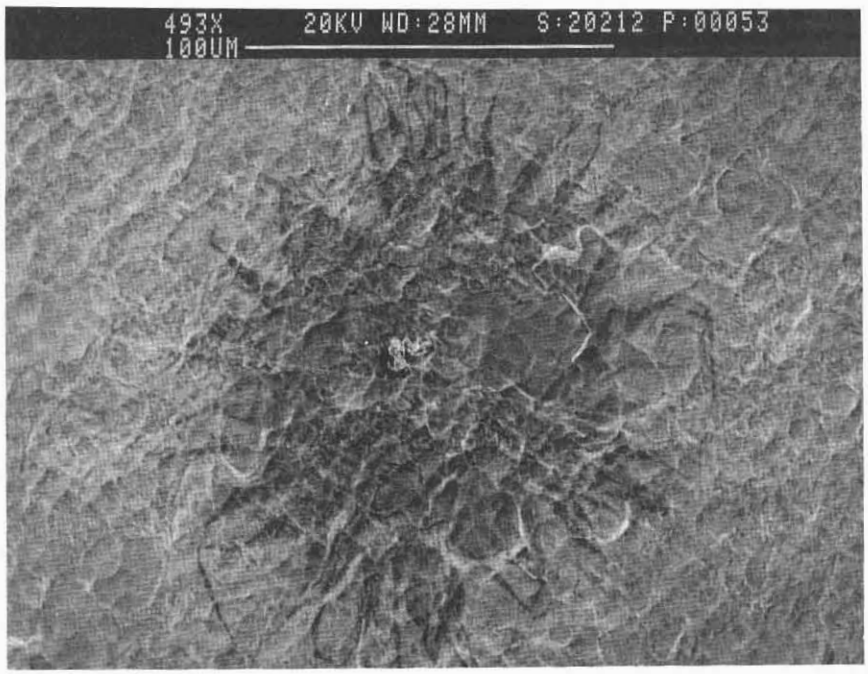

Figure 1a:
Scanning electron image of a starburst. Note the carbon flake at the center.

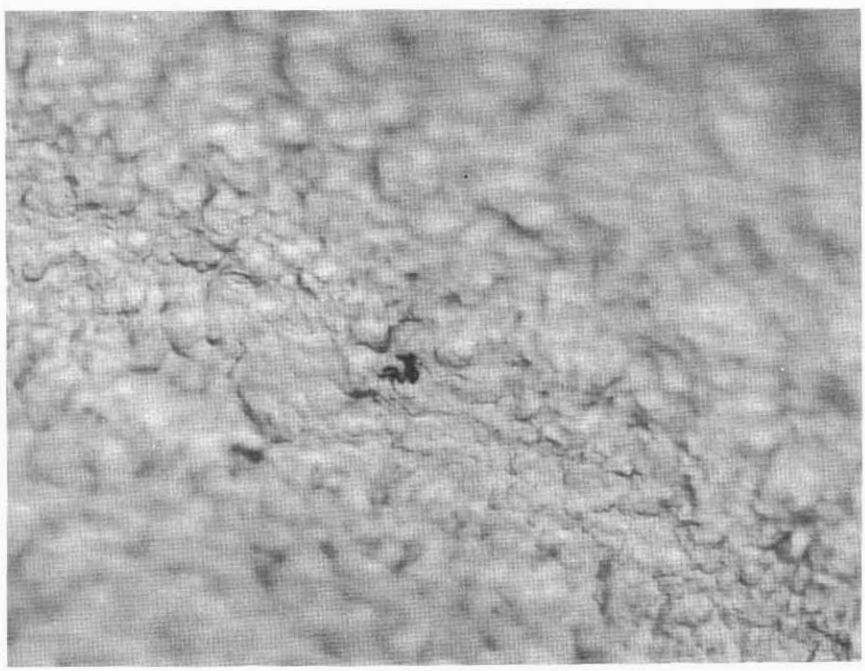

Figure 1b:
The region of 1a as seen in an optical microscope. The carbon flake can be seen but the starburst is not visible. Subsequent examination in an SEM showed the starburst to be still there.

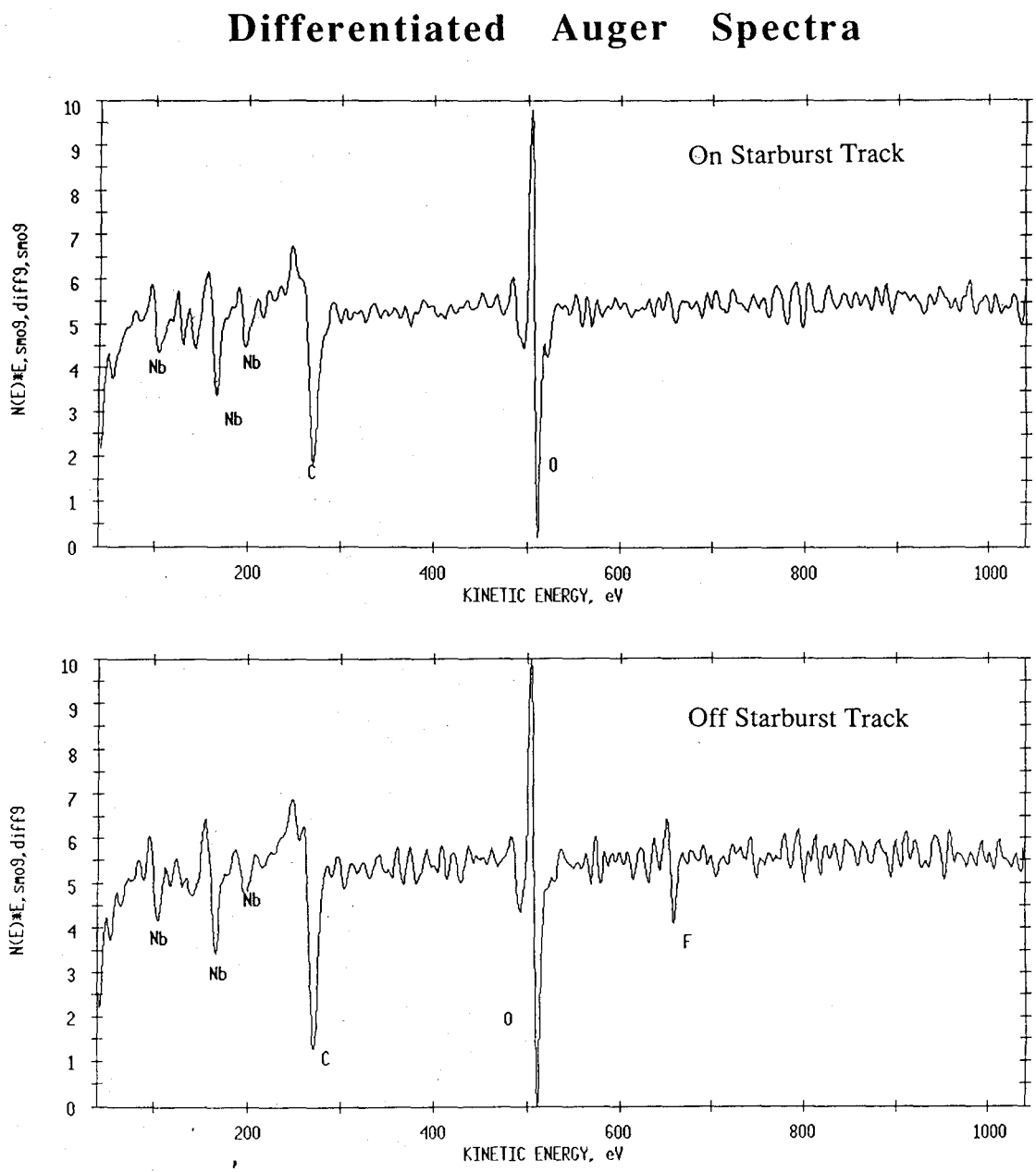

Figure 2:
Auger Electron spectra of regions just inside (top) and just outside (bottom) the track of a starburst. No fluorine is detected inside the track but fluorine is found outside..

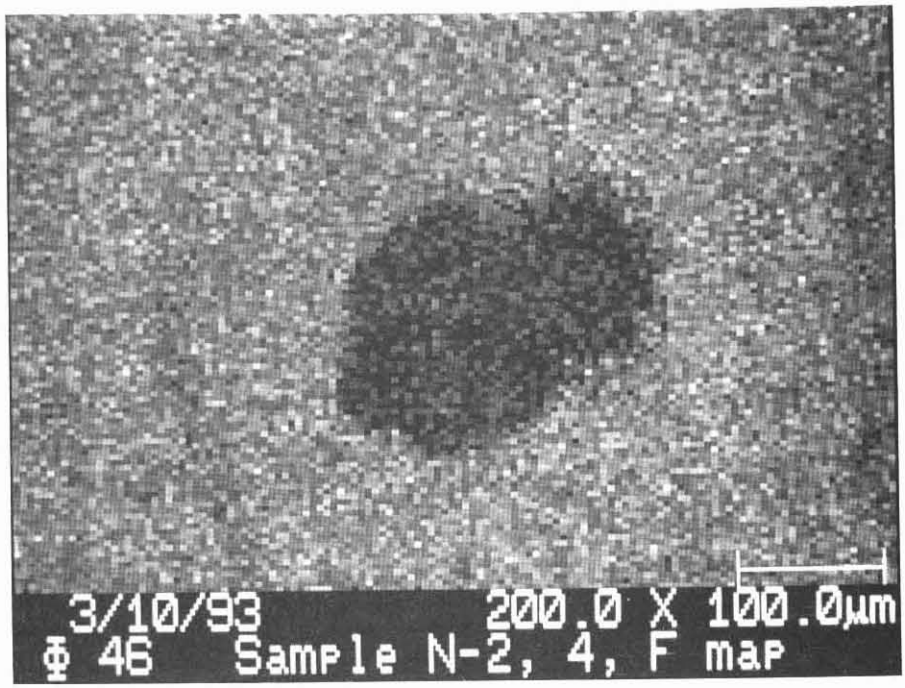

Figure 3a:
AES map for fluorine around the region of a starburst. The light regions are fluorine rich. There is a strong correspondence between the fluorine depleted regions and the location of the starburst imaged in 3b.

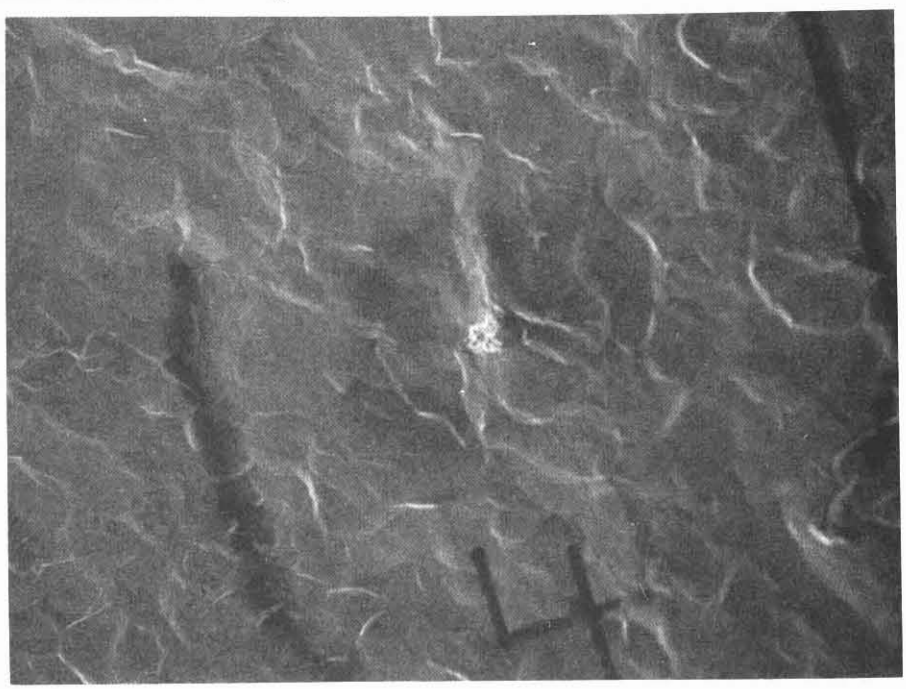

Figure 3b:
Scanning elctron reference for the map of 3a. The dark lines outside the starburst are from intentional electron beam markings of the surface to aide in locating the starbursts in the SEM of the AES system. These markngs also show fluorine depletion in 3a.

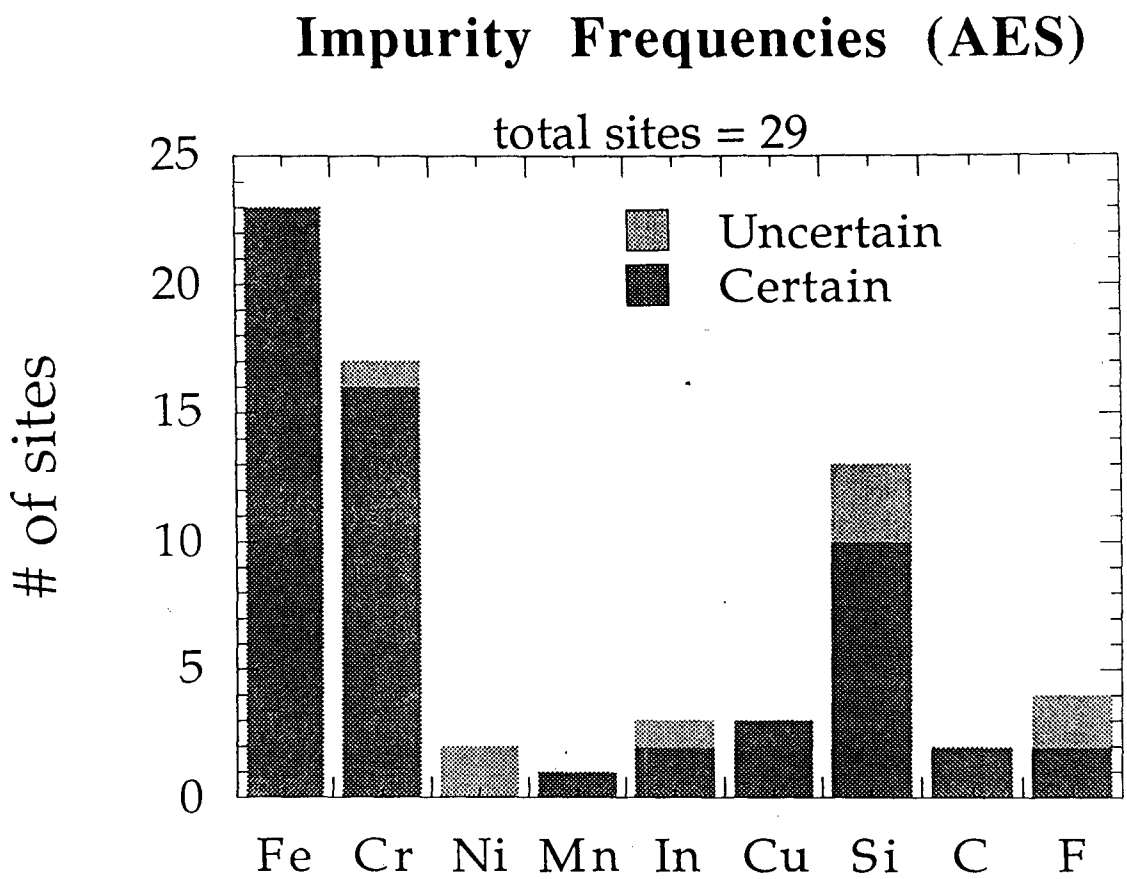

Figure 4:
Graph of the relative frequencies of occurance of the elements found in the AES analysis of two dimples. A primary impurity was found inside every starburst examined. Sometimes secondary impurities were detected. Sometimes the low concentration and/or the possibility of peak-overlap made identifiction of these secondary impurities difficult. These show up as "uncertain" in the statistics.

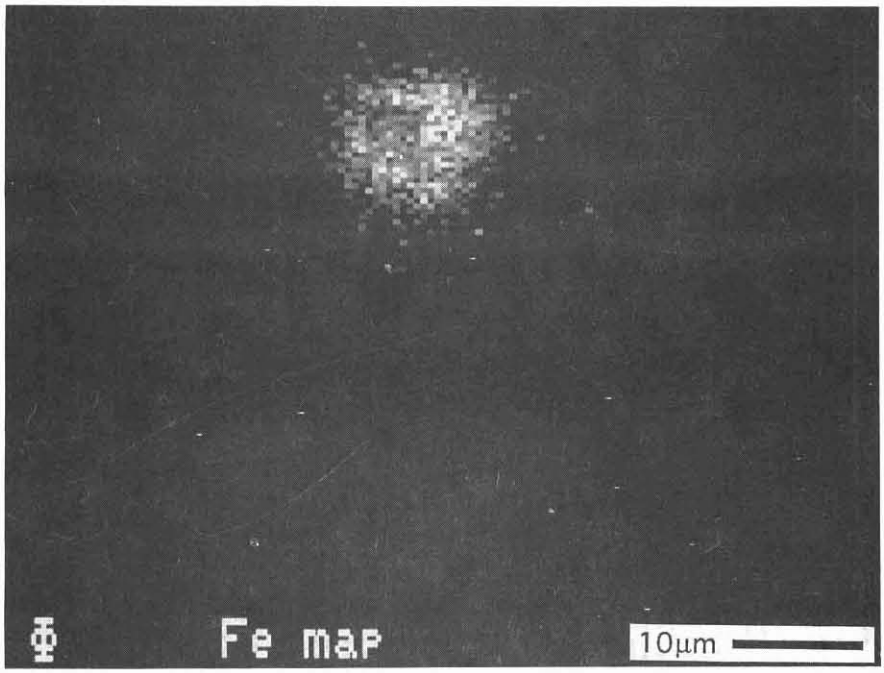

Figure 5a:
Iron map of a region containing two craters (SEI reference in 5b). Note that the iron extends beyond the edge of the crater. No impurity was detected in the second crater.

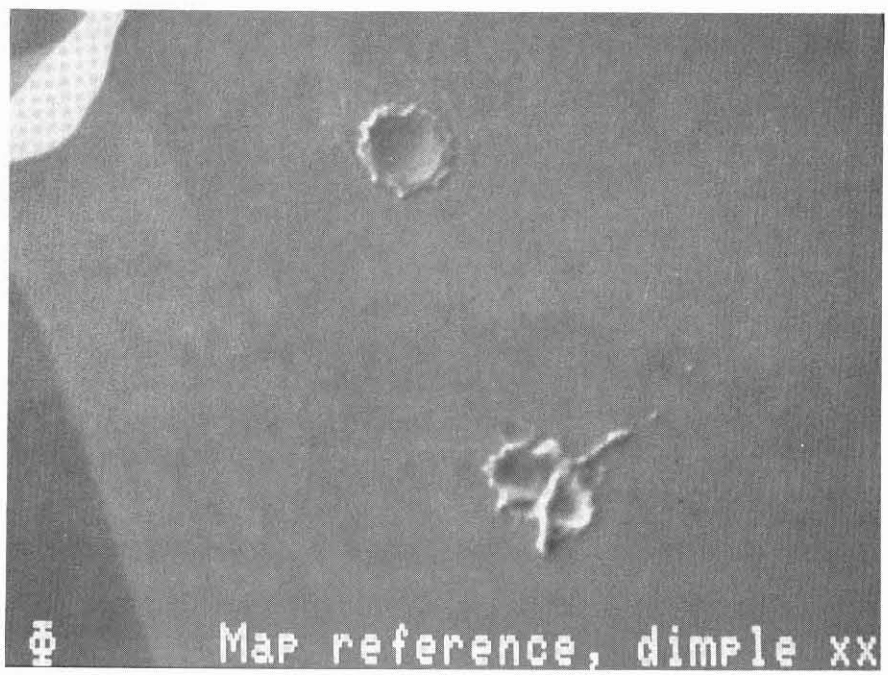

Figure 5b:
Secondary Electron Image of the region mapped in 5a.

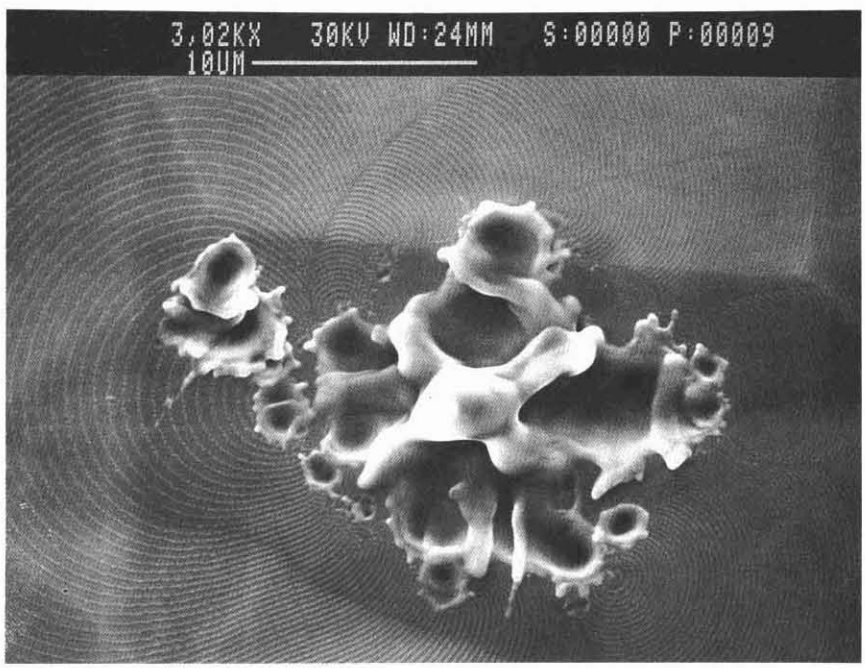

Figure 6
Cluster of craters at the center of a starburst. Note the many ripples associated with this area. Ripples are frequently seen in conjunction with molten craters like this. This area was examined by Atomic Force Microscopy.

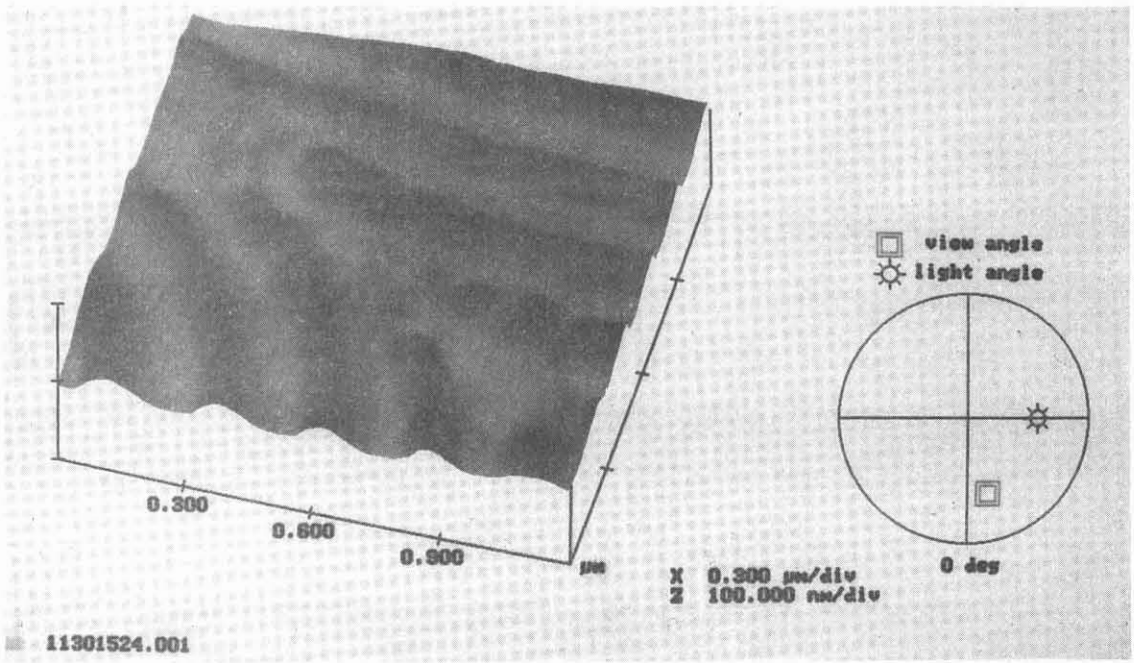

Figure 7

Perspective view of a boundary between wavetrains from different sources. There appears to be an enhanced tendency for wave crests to break up into nodules along such boudaries.

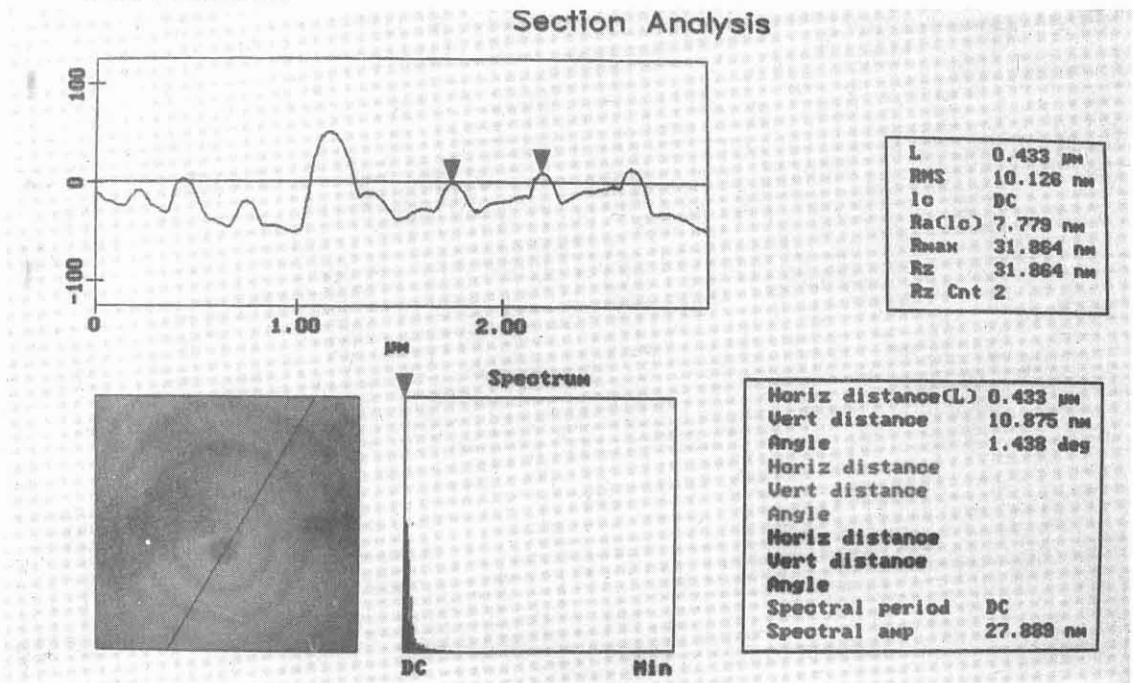

Figure 8:

Concentric ripple pattern from a source approx. 30nm from nearest crater. The profile is taken along the section line indicated in the grayscale image below it. There is a flake of material on the site which probably postdates formation of the pattern, since it seems to have no effect on ripple propagation.